Title

A [4Fe–4S]-Fe(CO)(CN)-l-cysteine intermediate is the first organometallic precursor in [FeFe] hydrogenase H-cluster bioassembly

Journal

Nature Chemistry, 10(5)

ISSN

1755-4330

Authors

Rao, Guodong
Tao, Lizhi
Suess, Daniel LM
et al.

Publication Date

2018-05-01

DOI

10.1038/s41557-018-0026-7

Peer reviewed

HHS Public Access

Author manuscript

Nat Chem. Author manuscript; available in PMC 2019 February 19.

Published in final edited form as:

Nat Chem. 2018 May ; 10(5): 555–560. doi:10.1038/s41557-018-0026-7.

A [4Fe-4S]-Fe(CO)(CN)-L-cysteine intermediate is the first organometallic precursor in [FeFe] hydrogenase H-cluster bioassembly

Guodong Rao[1], **Lizhi Tao**[1], **Daniel L. M. Suess**[1,2], and **R. David Britt**[1,*]

[1]Department of Chemistry, University of California, Davis, CA 95616, USA

[2]Current address: Department of Chemistry, Massachusetts Institute of Technology, Cambridge, MA 02139, USA

Abstract

Biosynthesis of the [FeFe] hydrogenase active site (the “H-cluster”) requires the interplay of multiple proteins and small molecules. Among them, the radical *S*-adenosyl-methionine enzyme HydG, a tyrosine lyase, has been proposed to generate an $Fe(CO)_2(CN)$ moiety-containing complex that is eventually incorporated into the H-cluster. Here we describe the characterization of an intermediate in the HydG reaction: a [4Fe-4S][(Cys)Fe(CO)(CN)] species, termed “Complex A”, in which a CO, a CN^- and a cysteine (Cys) molecule bind to the unique “dangler” Fe site of the auxiliary [5Fe-4S] cluster of HydG. Identification of this intermediate—the first organometallic precursor to the H-cluster—validates the previously hypothesized HydG reaction cycle and provides a basis for elucidating the biosynthetic origin of other moieties of the H-cluster.

Graphical Abstract:

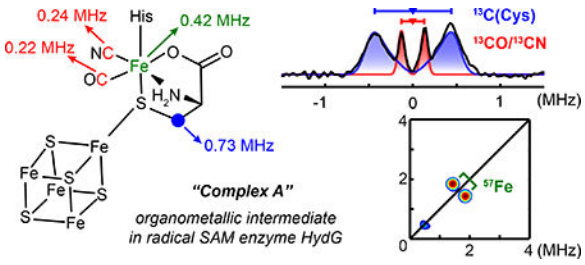

Biosynthesis of the [FeFe] hydrogenase active site H-cluster requires several Fe-S proteins that perform poorly understood reactions. Now, a reaction intermediate trapped in the enzyme HydG is shown to contain a [(Cys)Fe(CO)(CN)] species, the first organometallic Fe moiety en route to the catalytic H-cluster.

* rdbritt@ucdavis.edu.

Author Contribution

G.R., L.T., D.L.M.S., and R.D.B. designed the experiments. G.R., L.T. and D.L.M.S. performed the experiments and analyzed the data. All authors contributed to writing the manuscript.

[FeFe] hydrogenases catalyze the efficient interconversion between H_2 and H^+/e^- and are involved in many metabolic processes that balance the redox potentials in cells.[1] There is also considerable interest in their application in biofuel cells.[2,3] The active site of [FeFe] hydrogenases, the H-cluster, consists of a canonical cysteine (Cys)-bound $[4Fe\text{-}4S]_H$ subcluster linked to a $[2Fe]_H$ subcluster in which the two Fe centers are coordinated by CO, CN^-, and a bridging azadithiolate ligand (Fig. 1a).[4,5] The unique structural features and catalytic activity of the H-cluster have stimulated interest regarding its biosynthesis.[2,6–12] Recent studies have demonstrated that assembly of the $[2Fe]_H$ subcluster requires several iron-sulfur cluster-containing maturases: HydE, HydF, and HydG (Fig. 1a).[13–21] Among them, HydG is a bifunctional radical *S*-adenosyl-methionine (SAM) enzyme that cleaves its substrate tyrosine (Tyr) to generate CO and CN^- (Fig. 1b)[16,22–24] and forms an $Fe(CO)_2(CN)$ moiety-containing organometallic precursor that is eventually incorporated into the H-cluster (Fig. 1c).[25]

These two reactions are carried out by HydG using two Fe-S clusters with distinct roles.[8,16,24–30] A SAM-binding $[4Fe\text{-}4S]_{RS}$ (RS = radical SAM) cluster bound near the N-terminus initiates the radical chemistry that leads to Tyr cleavage. Upon one-electron reduction of the $[4Fe\text{-}4S]_{RS}$ cluster, SAM is cleaved to a 5'-dAdo radical, which likely abstracts an H atom from the amino group[31] of Tyr. This induces Cα-Cβ cleavage to give a 4-hydroxybenzyl radical (4-OB•),[27] along with dehydroglycine (DHG) which is in turn converted into CO and CN^- through mechanisms under investigation (Fig. 1b). Near the C-terminus, HydG harbors a unique [5Fe-4S] auxiliary cluster, recently identified by X-ray crystallographic analysis with support from biochemical and spectroscopic studies.[32] The auxiliary cluster contains a high spin "dangler" Fe^{2+} ($S = 2$) chelated by a bridging Cys molecule by which it is linked to a conventional $[4Fe\text{-}4S]^+$ cluster ($S = 1/2$) through the cysteine S, forming an $S = 5/2$ resting state in the reduced form (Fig. 1c).[32,33] The dangler Fe and the bridging Cys were shown to be labile towards chelating agents such as EDTA and CN^-.[32,33] Several species have been identified in the HydG reaction in addition to Tyr cleavage product (*p*-cresol): stopped-flow Fourier transform infrared (SF-FTIR) spectroscopic studies indicated the sequential formation of two CO/CN^--containing Fe complexes,[25] and electron paramagnetic resonance (EPR) spectroscopic studies revealed the presence of a $[4Fe\text{-}4S]_{aux}$-CN species with the synthon built upon the dangler Fe presumably released (Fig. 1c).[33]

Taken together, these results lead to a hypothesized mechanistic framework of HydG (Fig. 1c),[33] in which CO and CN^- bind to the dangler Fe in the auxiliary cluster to generate a discrete $[(Cys)Fe(CO)_2(CN)]^-$ complex as the reaction product. In this mechanism, it has been suggested that Cys serves, at a minimum, to deliver the $[Fe(CO)_2(CN)]^+$ moiety to the next maturase, and that the Cys ligand in this complex may be further processed to install the azadithiolate bridging ligand.[33] These proposals were supported by evidences that Cys binds the auxiliary [4Fe-4S] cluster,[33] and that Cys is required for generating organometallic $Fe(CO)_x(CN)_y$ intermediates.[34] However, it has not been demonstrated that the Cys-chelated dangler Fe is the site of organometallic complex formation; i.e., there has not been any direct observation of the proposed $[4Fe\text{-}4S][(Cys)Fe(CO)_x(CN)_y]$ species. We reasoned that the first organometallic intermediate proposed—[4Fe–4S][(Cys)Fe(CO)(CN)], termed "Complex A" (Fig. 1c)—could serve this purpose. In particular, we expected such a species

to adopt an $S = 1/2$ ground state in its reduced form, owing to the low spin $S = 0$ dangler Fe^{2+} that results from the binding of the strong field π-acid ligands CO and CN^-, leaving the $S = 1/2$ $[4Fe–4S]^+_{aux}$ cluster as the sole source of paramagnetism.

In this paper, we report the spectroscopic characterization of Complex A trapped during HydG turnover. The EPR spectroscopic studies herein establish the connectivity between the C-terminal auxiliary [4Fe-4S] cluster, the bridging Cys molecule, the dangler Fe, and the CO and CN^- ligands in Complex A, and thereby provide direct evidence that the first organometallic precursor to the H-cluster is a HydG-bound [4Fe-4S][(Cys)Fe(CO)(CN)] species. In addition, a dicyano analogue of Complex A, [4Fe-4S][(Cys)$Fe(CN)_2$], was generated non-enzymatically, which further demonstrates the formation of $Fe(CO)_x(CN)_y$ species on the dangler Fe site.

Results

Intermediates in the HydG reaction with one equivalent of Tyr.

When the HydG reaction was performed by using excess dithionite and SAM, but only one equivalent Tyr, and freeze-quenched at 24 s (the “standard condition”, see Methods), the resulting sample exhibited a complex set of signals near $g \sim 2$ in its continuous wave (CW)-EPR spectrum (Fig. 2a, top black trace). Simulation of this spectrum reveals three species (Fig. 2a, Supplementary Information): species **1** (red trace) with $g = [2.058, 1.922, 1.882]$ is assigned to Complex A for reasons we discuss below; species **2** (blue trace) with $g = [2.009, 1.881, 1.842]$ originates from the SAM-bound $[4Fe\text{-}4S]^+_{RS}$ cluster, as previously established;[26,27] and species **3** (green trace) with $g = [2.044, 1.942, 1.904]$, the origin of which is currently unknown. The spectral composition of the 24 s reaction sample was further confirmed by deconvolution of its Q-band electron spin-echo detected EPR spectrum (Fig. 2b) and the corresponding pseudo-modulated spectrum (Supplementary Fig. 1).

In determining the identity of species **1**, we considered the following observations. First, the intensity of EPR signal from species **1** decreases as the reaction proceeds (Supplementary Fig. 2 and 3), which is consistent with the kinetics of Complex A in our previous SF-FTIR studies.[25] Second, the intensity of this signal also decreases with increasing equivalents of Tyr (Supplementary Fig. 4), which explains why it was not as obvious in previous studies in which 10~15 equivalents of Tyr were used.[27] Third, the temperature profile of species **1** is similar to that of a typical $S = 1/2$ $[4Fe\text{-}4S]^+$ cluster (Supplementary Fig. 5). Fourth, compared in Supplementary Table 1 are the g tensors for several HydG auxiliary cluster-derived species. The g tensor of species **1** is distinct from that of the resting state of HydG auxiliary cluster that has a ground state of $S = 5/2$ ($g_{eff} = [9.5, 4.7, 4.1, 3.7]$). It is also different from two other $S = 1/2$ species observed previously: the cyanide bound HydG auxiliary cluster ($[4Fe\text{-}4S]^+_{aux}$-CN, $g = [2.09, 1.94, 1.93]$) observed in the prolonged reaction (20 min) sample,[32,33] and the dangler Fe-deficient HydG auxiliary cluster ($[4Fe\text{-}4S]^+_{aux}$-Cys, $g = [2.064, 1.895, 1.865]$).[33] These facts suggest that species **1** could be Complex A. In what follows, we test this hypothesis by employing electron nuclear double resonance (ENDOR) and hyperfine sublevel correlation (HYSCORE) spectroscopy to probe the structure/ligand environment of species **1** using isotopically labeled Tyr (^{13}C and ^{15}N), Cys (3-^{13}C), and Fe (^{57}Fe).

$^{13}CO/^{13}C^{15}N$ in Complex A.

HydG-catalyzed cleavage of isotopically labeled Tyr (^{13}C and ^{15}N) generates $^{13}C/^{15}N$ labeled $Fe(CO)_x(CN)_y$ intermediates (Fig. 1c and Fig. 3a).[25,33] In $Fe(CO)_x(CN)_y$ intermediates, the dangler Fe to which CO and CN^- are bound is proposed to be a diamagnetic, low spin Fe^{2+} center; as such, the electron spin density is expected to reside primarily on the $[4Fe\text{-}4S]^+_{aux}$ cluster, and the ^{13}CO, ^{13}CN, $C^{15}N$ hyperfine coupling interactions (HFI) are expected to be small, making these $I = 1/2$ nuclei good targets for Mims-ENDOR (Supplementary Methods).

The Mims-ENDOR spectrum recorded at $g = 1.922$ of a sample generated under the standard condition (*vide supra*) using U-$^{13}C_9$-Tyr as the substrate exhibited a sharp doublet centered at the Larmor frequency of ^{13}C, with a splitting of ~0.27 MHz (Fig. 3b). To clarify which EPR species contribute to the ^{13}C ENDOR signals, we collected field-dependent ^{13}C Mims-ENDOR spectra (Fig. 3b) under optimized conditions (Supplementary Fig. 6), at field positions indicated by the arrows shown in Fig. 2b. Mims-ENDOR signals (Fig. 3b) were not observed at $g = 1.851$ (the rightmost arrow, Fig. 2b) where only species **2** (SAM-bound $[4Fe\text{-}4S]^+_{RS}$ cluster) is present, but were observed at $g = 1.882$ (the second rightmost arrow, Fig. 2b) where both species **1** and **2** are present while species **3** is not present (Fig. 3b), clearly indicating that these ENDOR signals arise from species **1**. Consistent with this assignment, the ^{13}C Mims-ENDOR signals were observed across the absorption envelope of species **1** (Fig. 2b, $g = 2.055$ to 1.882; Fig. 3b).

To clarify which carbon(s) in Tyr give rise to the observed ^{13}C ENDOR signals, we prepared reaction samples under the standard condition using selectively ^{13}C-labeled Tyr, specifically either 1-^{13}C-Tyr which generates ^{13}CO, or 2-^{13}C-Tyr which generates $^{13}CN^-$ (Fig. 3a). Interestingly, ^{13}C Mims-ENDOR spectra of these two samples recorded at g_2 (1.922) of species **1** were nearly indistinguishable, and the signals were not observed when SAM is not present (Supplementary Fig. 7), ruling out its origin from any unreacted Tyr species bound to the clusters. Further field-dependent ^{13}C Mims-ENDOR measurements indicate that the HFI from ^{13}CO ([0.10, 0.30, 0.27] MHz, Fig. 3c) and $^{13}CN^-$ ([0.15, 0.30, 0.28] MHz, Fig. 3d) are almost identical, and that they both contribute to the ENDOR spectra in Fig. 3a where both ^{13}CO and $^{13}CN^-$ HFI are detected. Based on these ^{13}C Mims-ENDOR experiments, we conclude that species **1** corresponds to Complex A as observed by FTIR spectroscopic studies.[25]

We also looked for the evidence for $C^{15}N^-$ binding to the dangler Fe by probing the ^{15}N HFI (generated from [U-$^{13}C_9$, ^{15}N]-Tyr). The small ^{15}N HFI, observed in X-band HYSCORE spectra of the reaction sample (Supplementary Fig. 8), further supports our assignment of species **1** as Complex A.

Bridging Cys molecule in Complex A.

Having assigned species **1** to Complex A, we then looked for evidence of the bridging Cys in this species. To this end, we selectively installed 3-^{13}C-Cys in the bridging position of the auxiliary [5Fe-4S] cluster of HydG using our previously established protocol (Fig. 3a, see Methods).[33] When the reaction was performed using this 3-^{13}C-Cys_{bridge}-labeled HydG and

U-$^{13}C_9$-Tyr at standard condition, the ^{13}C Mims-ENDOR spectra of the resulting sample showed the same small ^{13}C HFI (a_{iso} = 0.23 MHz, Fig. 3e, red trace) from $^{13}CO/^{13}CN$, as observed with unlabeled HydG (Fig. 3b, *vide supra*). In addition, a second set of ^{13}C ENDOR signals with a larger hyperfine splitting was observed (Fig. 3e, simulated with blue trace), which must originate from the labeled ^{13}C on the bridging Cys. A similar field-dependent ^{13}C Mims-ENDOR study (*vide supra*) reveals that this set of signals appears concurrently with the $^{13}CO/^{13}CN^-$ signals (Fig. 3e, from g = 2.055 to g = 1.882), which indicates that it also originates from species **1**, i.e., Complex A.

The ENDOR of 3-^{13}C-Cys_{bridge} in Complex A can be simulated using a ^{13}C hyperfine tensor of A = [1.00, 0.20, 1.00] MHz (Fig. 3e, blue trace), with a_{iso} = 0.73 MHz and T = −0.27 MHz (sign relative to a_{iso}). Importantly, this ^{13}C HFI is distinct from that reported for the Cys-bound HydG auxiliary cluster, $[4Fe\text{-}4S]^+_{aux}$-[3-^{13}C-Cys] (A = [0.83, 0.83, 1.03] MHz).[33] The dipolar component of this ^{13}C HFI in Complex A ($|T|$ = 0.27 MHz) approximately corresponds to a distance between the labeled carbon and the nearest Fe in the $[4Fe\text{-}4S]_{aux}$ cluster of ~4 Å (Supplementary Information). This distance is broadly consistent with the proposed structure of Complex A in which the Cys C3 carbon is separated from the [4Fe-4S] cluster by a bridging thiolate sulfur atom.

Dangler ^{57}Fe in Complex A.

We next sought to verify the presence of the dangler Fe in Complex A and to clarify its spin state by measuring the ^{57}Fe HFI. A sample of $^{57}Fe_{dangler}$-labeled HydG was generated using a previous established protocol[33] (Fig. 3a) and was subjected to the standard reaction conditions to generate the $^{57}Fe_{dangler}$-labeled Complex A (Fig. 4c). The Q-band HYSCORE spectrum of this sample collected at g = 2.05 reveals crosspeaks on the antidiagonal line centered at the ^{57}Fe Larmor frequency (1.63 MHz at 1186 mT, Fig. 4a). These signals are not present in the corresponding natural abundance spectrum recorded under the same conditions (Fig. 4b) and must therefore be attributed to the dangler ^{57}Fe.

Field-dependent HYSCORE spectra were collected and simulated to extract the ^{57}Fe HFI tensor, which is nearly isotropic with A = [0.45, 0.30, 0.50] MHz, a_{iso} = 0.42 MHz, and a major $|T|$ ~ 0.07 MHz (Fig. 4d). The spin density on the dangler ^{57}Fe is estimated as follows:[35] a Fermi contact (a_{iso}) of 0.42 MHz corresponds to 0.056% spin density in the 4s orbital, and the anisotropic contribution ($|T|$ ~ 0.067 MHz) gives a spin density of 0.24% in 3d orbitals, adding up to a total spin density of ~0.3% on the dangler ^{57}Fe. The small ^{57}Fe spin density validates the diamagnetic nature of the dangler Fe upon binding to CO/CN^-, and is consistent with the small ^{13}C HFI detected for $^{13}CO/^{13}CN^-$. In the point dipole approximation, the dipolar part of ^{57}Fe HFI corresponds to a distance between the dangler Fe and the nearest Fe in the [4Fe-4S] cluster of ~4 Å (Supplementary Information). For comparison, the same distance in the X-ray crystal structure of HydG is 4.1 Å (PDB ID code: 4WCX[32]). Due to the likely structural changes upon CO/CN^- binding (and the bridging Cys molecule was absent in the X-ray structure), this HYSCORE-derived distance is reasonably consistent with the X-ray crystallographic structure, and it suggests that the dangler Fe is close to the $[4Fe\text{-}4S]_{aux}$ cluster in Complex A.

The ^{57}Fe we observed in Complex A has the smallest ^{57}Fe HFI that has been reported to date. A few other examples of weak ^{57}Fe HFI are summarized in Table 1: a reaction intermediate of LipA has ^{57}Fe a_{iso} = 1–2 MHz between a formally diamagnetic $[4Fe\text{-}4S]^{2+}$ cluster and an carbon-centered organic radical;[36] the distal Fe in the H_{ox}-CO state of [FeFe] hydrogenase H-cluster has ^{57}Fe a_{iso} = 0.8 MHz (from *Desulfovibrio desulfuricans* DdH[37]) or 1.3 MHz (from *Chlamydomonas reinhardtii* HydA1[38] reconstituted with synthetic $[^{57}Fe_2(adt)(CO)_4(CN)_2]^{2-}$); the Ni-A, Ni-B and Ni-C states in [NiFe] hydrogenase from *Desulfovibrio gigas* have ^{57}Fe a_{iso} = 0.8–1.4 MHz between a formally diamagnetic Fe^{2+} and the Ni center.[39,40] In all cases, the ^{57}Fe coupled to paramagnetic centers are either formally diamagnetic, or have very small spin density.

Taken together, the ^{13}C and ^{57}Fe HFI values demonstrate that Complex A is comprised of a low-spin dangler Fe^{2+} center bound to a CO and a CN^-, and that it is covalently linked to the $[4Fe\text{-}4S]_{aux}$ cluster through a bridging Cys molecule. Clarifying the structure of this intermediate provides direct evidence that HydG generates $[Cys][Fe(CO)_x(CN)_y]$ species as the reaction product(s). Interestingly, Complex A is an unusual $S = 1/2$ [5Fe-4S] cluster, with the only similar example being the sirohaem-[5Fe-4S] cluster in which the sirohaem iron (with CO or CN^- bound) is weakly coupled to a [4Fe-4S] cluster through a bridging Cys residue.[41–43] In this regard, Complex A also shares some similarity with the recently identified hydride state (H_{hyd}) of the [FeFe] hydrogenase in which two low-spin Fe^{2+} centers are linked to a paramagnetic $[4Fe\text{-}4S]^+$ cluster through a bridging Cys residue.[44–46]

Dicyano analogue of Complex A.

We further tested the possibility of generating Complex A and its analogs in non-enzymatic manners, that is, by incubating HydG with CO and/or CN^- and comparing the corresponding EPR signals to species **1**. Although such attempts to generate Complex A have not yet proven fruitful, we were able to generate a cyanide adduct of HydG (Fig. 5a). In a cyanide titration experiment, we observed a new $S = 1/2$ species on CW-EPR upon addition of 12 eq. of $K^{13}CN$ to HydG, and the signal intensity reached a maximum when 50 eq. of $K^{13}CN$ was added (Supplementary Fig. 9). The CW-EPR spectrum of the "HydG + 50 eq. $K^{13}CN$" sample is simulated with three species, the most abundant new species among which (Fig. 5b, red trace) has g = [2.054, 1.927, 1.879], almost identical to that of Complex A (Supplementary Table 1). Based on this g tensor similarity, we tentatively assigned this EPR species to the dicyano analog of Complex A, $[4Fe\text{-}4S][(Cys)Fe(CN)_2]$ (Fig. 5a), though a [4Fe-4S][(Cys)Fe(CN)(L)] structure cannot be ruled out (L is a different ligand that completes the octahedral coordination sphere of the dangler Fe). $^{13}CN^-$ binding to dangler Fe was further ascertained by field-dependent ^{13}C Mims-ENDOR studies (Fig. 5c). The observed ENDOR signals, simulated with a ^{13}C HFI of A = [0.20, 0.30, 0.30] MHz (Fig. 5c, red trace), are also similar to the $^{13}CO/^{13}CN^-$ signals in Complex A, but distinct from that in the previously reported $[4Fe\text{-}4S]_{aux}$-^{13}CN species (A = [−5.0 −4.0 0.9] MHz).[32] Observation of this cyanide adduct provides further evidence that the dangler Fe site is involved in the formation of $Fe(CO)_x(CN)_y$ species.

Discussion

Using insights from previous work and results in this study, the molecular-level mechanism of H-cluster biosynthesis may be summarized as follows. The radical SAM cluster of HydG initiates cleavage of Tyr into *p*-cresol and DHG—a CO/CN^- precursor. At the auxiliary cluster of HydG, CO/CN^- add to a dangler Fe to generate a [4Fe-4S][(Cys)Fe(CO)(CN)] intermediate, as demonstrated here. A second Tyr cleavage-generated CO/CN^- pair further converts this intermediate into a $[Fe(CO)_2(CN)]$-moiety containing complex, proposed to be $[(Cys)Fe(CO)_2(CN)]$. Two equivalents of the latter Fe complex may be processed by HydE to generate the azadithiolate bridging ligand from the bound Cys fragment, followed by further processing on HydF to form the H-cluster-like 2Fe precursor. Alternatively, the azadithiolate ligand may be sourced from other molecular precursors. At the end of this cascade, HydF is thought to deliver a 2Fe subcluster to apo-hydrogenase to give active hydrogenase.

Many important questions about this process remain, including to which maturase enzyme the $[(Cys)Fe(CO)_2(CN)]$ complex is delivered; how the azadithionate bridge is formed and whether the HydG-derived $[(Cys)Fe(CO)_2(CN)]$ is a precursor to it; and at what point the first 2Fe center is formed. The results reported here provide a useful foundation for studying these important problems by definitively showing that HydG generates [Cys] $[Fe(CO)_x(CN)_y]$ species. Further deploying these *in vitro* selective isotope-labeling strategies and advanced spectroscopic methods should enable additional mechanistic insights to be gleaned.

Methods

Generation of 3-^{13}C-Cys$_{bridge}$ and ^{57}Fe$_{dangler}$ labeled HydG.

This procedure is essentially the same to that for labeling the dangler Fe reported previously.[33] As-isolated HydG was concentrated to ~300 μM. Sodium dithionite, SAM, 3-^{13}C-Cys was added to 3 mM, and EDTA to 600 μM (in that order). This mixture was incubated for 10 min at room temperature, diluted by 10-fold with a buffer containing 3 mM dithionite, SAM and 3-^{13}C-Cys, and concentrated to the original volume by using 30 kDa cutoff Amicon centrifugal filters. To the dangler Fe-removed protein was then added $^{57}Fe^{2+}$ (see Supplementary Methods) to a final concentration of ~1 mM. This labeled protein sample was used immediately for HydG reactions.

The “standard condition” to generate HydG reaction mixture containing Complex A

As-isolated or labeled HydG was concentrated to ~800 μM. SAM and dithionite was added to a final concentration of ~8 mM. The reaction was initiated by transferring 60 μL of this solution into an EPR sample tube (Ka-band quartz tube with an outer diameter of 2.4 mm and inner diameter of 2.0 mm) and mixing with 10 μL of 5 mM Tyr (labeled as desired) at the bottom of the EPR tube. The final concentrations for HydG and Tyr were ~700 μM. For X-band samples, a 150 μL protein solution was mixed with 25 μL Tyr in an X-band tube. The reaction was mixed quickly by pipetting up and down once, rapidly transferred outside of the glovebox and freeze-quenched at different time points. With this procedure, we were

able to quench the reaction as early as 24 s. The EPR samples were stored in liquid nitrogen prior to analysis.

Generation of the di-CN analogue of Complex A.

As-isolated HydG was concentrated to ~600 μM. Sodium dithionite and SAM were added to a final concentration of 6 mM. To 50 μL of the enzyme solution was added 10 μL 60 mM $K^{13}CN$ solution. After brief mixing, the solution was transferred to EPR sample tubes mentioned above and frozen in liquid nitrogen prior to analysis.

Data availability.

The data collected in this study are available from the corresponding author upon request (including data presented in the main text and in the Supplementary Information).

Supplementary Material

Refer to Web version on PubMed Central for supplementary material.

Acknowledgment

We thank James Swartz from Stanford University for providing the *E. coli* strain overexpressing *So*HydG. This work is supported by National Institute of Health (GM104543). Correspondence and requests for materials should be addressed to R.D.B. The authors declare no competing financial interests.

References

1. Vignais PM & Billoud B Occurrence, classification, and biological function of hydrogenases: an overview. Chem. Rev 107, 4206–4272 (2007). [PubMed: 17927159]
2. Lubitz W, Ogata H, Rudiger O & Reijerse E Hydrogenases. Chem. Rev 114, 4081–4148 (2014). [PubMed: 24655035]
3. Barber J & Tran PD From natural to artificial photosynthesis. J. Royal Soc. Interface 10, 20120984 (2013).
4. Peters JW, Lanzilotta WN, Lemon BJ & Seefeldt LC X-ray crystal structure of the Fe-only hydrogenase (CpI) from Clostridium pasteurianum to 1.8 angstrom resolution. Science 282, 1853–1858 (1998). [PubMed: 9836629]
5. Nicolet Y, Piras C, Legrand P, Hatchikian CE & Fontecilla-Camps JC Desulfovibrio desulfuricans iron hydrogenase: the structure shows unusual coordination to an active site Fe binuclear center. Structure 7, 13–23 (1999). [PubMed: 10368269]
6. Broderick JB et al. H-cluster assembly during maturation of the [FeFe]-hydrogenase. J. Biol. Inorg. Chem 19, 747–757 (2014). [PubMed: 24972661]
7. Vincent KA, Parkin A & Armstrong FA Investigating and exploiting the electrocatalytic properties of hydrogenases. Chem. Rev 107, 4366–4413 (2007). [PubMed: 17845060]
8. Suess DL, Kuchenreuther JM, De La Paz L, Swartz JR & Britt RD Biosynthesis of the [FeFe] hydrogenase H cluster: A central role for the radical SAM enzyme HydG. Inorg. Chem 55, 478–487 (2016). [PubMed: 26703931]
9. Birrell JA, Rüdiger O, Reijerse EJ & Lubitz W Semisynthetic hydrogenases propel biological energy research into a new era. Joule 1, 61–76 (2017).
10. Shepard EM et al. [FeFe]-hydrogenase maturation. Biochemistry 53, 4090–4104 (2014). [PubMed: 24878200]
11. Peters JW et al. [FeFe]- and [NiFe]-hydrogenase diversity, mechanism, and maturation. Biochim. Biophys. Acta 1853, 1350–1369 (2015). [PubMed: 25461840]

12. Mulder DW et al. Insights into [FeFe]-hydrogenase structure, mechanism, and maturation. Structure 19, 1038–1052 (2011). [PubMed: 21827941]
13. Boyer ME, Stapleton JA, Kuchenreuther JM, Wang CW & Swartz JR Cell-free synthesis and maturation of [FeFe] hydrogenases. Biotechnol. Bioeng 99, 59–67 (2008). [PubMed: 17546685]
14. Posewitz MC et al. Discovery of two novel radical S-adenosylmethionine proteins required for the assembly of an active [Fe] hydrogenase. J. Biol. Chem 279, 25711–25720 (2004). [PubMed: 15082711]
15. McGlynn SE et al. HydF as a scaffold protein in [FeFe] hydrogenase H-cluster biosynthesis. FEBS Lett. 582, 2183–2187 (2008). [PubMed: 18501709]
16. Pilet E et al. The role of the maturase HydG in [FeFe]-hydrogenase active site synthesis and assembly. FEBS Lett. 583, 506–511 (2009). [PubMed: 19166853]
17. Mulder DW et al. Activation of HydA(DeltaEFG) requires a preformed [4Fe-4S] cluster. Biochemistry 48, 6240–6248 (2009). [PubMed: 19435321]
18. Mulder DW et al. Stepwise [FeFe]-hydrogenase H-cluster assembly revealed in the structure of HydA(DeltaEFG). Nature 465, 248–251 (2010). [PubMed: 20418861]
19. Shepard EM et al. Synthesis of the 2Fe subcluster of the [FeFe]-hydrogenase H cluster on the HydF scaffold. Proc. Natl. Acad. Sci. U. S. A 107, 10448–10453 (2010). [PubMed: 20498089]
20. Kuchenreuther JM, Britt RD & Swartz JR New insights into [FeFe] hydrogenase activation and maturase function. PLoS One 7, e45850 (2012). [PubMed: 23049878]
21. Berto P et al. The [4Fe-4S]-cluster coordination of [FeFe]-hydrogenase maturation protein HydF as revealed by EPR and HYSCORE spectroscopies. Biochim. Biophys. Acta 1817, 2149–2157 (2012). [PubMed: 22985598]
22. Kuchenreuther JM, George SJ, Grady-Smith CS, Cramer SP & Swartz JR Cell-free H-cluster synthesis and [FeFe] hydrogenase activation: all five CO and CN(−) ligands derive from tyrosine. PLoS One 6, e20346 (2011). [PubMed: 21673792]
23. Driesener RC et al. [FeFe]-hydrogenase cyanide ligands derived from S-adenosylmethionine-dependent cleavage of tyrosine. Angew. Chem. Int. Ed. Engl 49, 1687–1690 (2010). [PubMed: 20108298]
24. Shepard EM et al. [FeFe]-hydrogenase maturation: HydG-catalyzed synthesis of carbon monoxide. J. Am. Chem. Soc 132, 9247–9249 (2010). [PubMed: 20565074]
25. Kuchenreuther JM et al. The HydG enzyme generates an Fe(CO)2(CN) synthon in assembly of the FeFe hydrogenase H-cluster. Science 343, 424–427 (2014). [PubMed: 24458644]
26. Driesener RC et al. Biochemical and kinetic characterization of radical S-adenosyl-L-methionine enzyme HydG. Biochemistry 52, 8696–8707 (2013). [PubMed: 24206022]
27. Kuchenreuther JM et al. A radical intermediate in tyrosine scission to the CO and CN^- ligands of FeFe hydrogenase. Science 342, 472–475 (2013). [PubMed: 24159045]
28. Rubach JK, Brazzolotto X, Gaillard J & Fontecave M Biochemical characterization of the HydE and HydG iron-only hydrogenase maturation enzymes from Thermatoga maritima. FEBS Lett. 579, 5055–5060 (2005). [PubMed: 16137685]
29. Nicolet Y et al. Crystal structure of HydG from Carboxydothermus hydrogenoformans: a trifunctional [FeFe]-hydrogenase maturase. ChemBioChem 16, 397–402 (2015). [PubMed: 25504963]
30. Pagnier A, Martin L, Zeppieri L, Nicolet Y & Fontecilla-Camps JC CO and CN^- syntheses by [FeFe]-hydrogenase maturase HydG are catalytically differentiated events. Proc. Natl. Acad. Sci. U. S. A 113, 104–109 (2016). [PubMed: 26699472]
31. Nicolet Y, Zeppieri L, Amara P & Fontecilla-Camps JC Crystal structure of tryptophan lyase (NosL): evidence for radical formation at the amino group of tryptophan. Angew. Chem. Int. Ed. Engl 53, 11840–11844 (2014). [PubMed: 25196319]
32. Dinis P et al. X-ray crystallographic and EPR spectroscopic analysis of HydG, a maturase in [FeFe]-hydrogenase H-cluster assembly. Proc. Natl. Acad. Sci. U. S. A 112, 1362–1367 (2015). [PubMed: 25605932]
33. Suess DL et al. Cysteine as a ligand platform in the biosynthesis of the FeFe hydrogenase H cluster. Proc. Natl. Acad. Sci. U. S. A 112, 11455–11460 (2015). [PubMed: 26324916]

34. Suess DL et al. The radical SAM enzyme HydG requires cysteine and a dangler iron for generating an organometallic precursor to the [FeFe]-hydrogenase H-cluster. J. Am. Chem. Soc 138, 1146–1149 (2016). [PubMed: 26764535]
35. Morton JR & Preston KF Atomic parameters for paramagnetic resonance data. J. Magn. Reson 30, 577–582 (1978).
36. Lanz ND et al. Characterization of a radical intermediate in lipoyl cofactor biosynthesis. J. Am. Chem. Soc. 137, 13216–13219 (2015). [PubMed: 26390103]
37. Silakov A, Reijerse EJ, Albracht SP, Hatchikian EC & Lubitz W The electronic structure of the H-cluster in the [FeFe]-hydrogenase from Desulfovibrio desulfuricans: a Q-band ^{57}Fe-ENDOR and HYSCORE study. J. Am. Chem. Soc 129, 11447–11458 (2007). [PubMed: 17722921]
38. Gilbert-Wilson R et al. Spectroscopic investigations of [FeFe] hydrogenase maturated with [57Fe2(adt)(CN)2(CO)4]2-. J. Am. Chem. Soc 137, 8998–9005 (2015). [PubMed: 26091969]
39. Carepo M et al. 17O ENDOR detection of a solvent-derived Ni-(OHx)-Fe bridge that is lost upon activation of the hydrogenase from Desulfovibrio gigas. J. Am. Chem. Soc 124, 281–286 (2002). [PubMed: 11782180]
40. Pandelia ME, Ogata H & Lubitz W Intermediates in the catalytic cycle of [NiFe] hydrogenase: functional spectroscopy of the active site. ChemPhysChem 11, 1127–1140 (2010). [PubMed: 20301175]
41. Christner JA, Janick PA, Siegel LM & Munck E Mössbauer studies of Escherichia coli sulfite reductase complexes with carbon monoxide and cyanide. Exchange coupling and intrinsic properties of the [4Fe-4S] cluster. J. Biol. Chem 258, 11157–11164 (1983). [PubMed: 6309834]
42. Krueger RJ & Siegel LM Spinach siroheme enzymes: Isolation and characterization of ferredoxin-sulfite reductase and comparison of properties with ferredoxin-nitrite reductase. Biochemistry 21, 2892–2904 (1982). [PubMed: 7104302]
43. Krueger RJ & Siegel LM Evidence for siroheme-Fe_4S_4 interaction in spinach ferredoxin-sulfite reductase. Biochemistry 21, 2905–2909 (1982). [PubMed: 6285956]
44. Winkler M et al. Accumulating the hydride state in the catalytic cycle of [FeFe]-hydrogenases. Nat. Commun 8, 16115 (2017). [PubMed: 28722011]
45. Mulder DW, Guo Y, Ratzloff MW & King PW Identification of a catalytic iron-hydride at the H-cluster of [FeFe]-hydrogenase. J. Am. Chem. Soc 139, 83–86 (2017). [PubMed: 27973768]
46. Reijerse EJ et al. Direct observation of an iron-bound terminal hydride in [FeFe]-hydrogenase by nuclear resonance vibrational spectroscopy. J. Am. Chem. Soc 139, 4306–4309 (2017). [PubMed: 28291336]

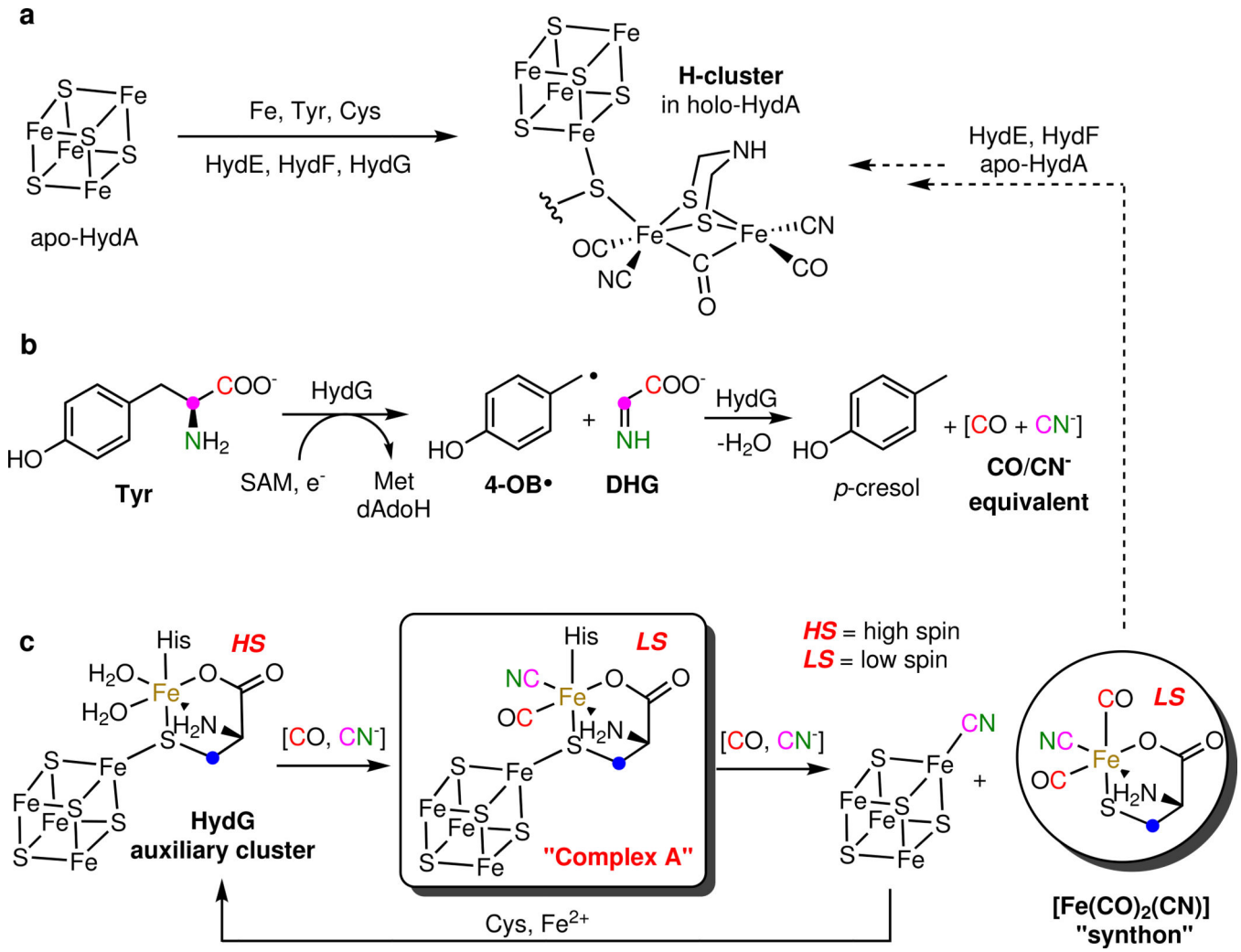

Figure 1.

[FeFe] hydrogenase (HydA) H-cluster bioassembly. **a**, Maturation of apo-HydA. **b**, Proposed mechanism by which the radical SAM cluster of HydG cleaves Tyr into CO and CN^{-}. **c**, Proposed mechanism by which the auxiliary cluster of HydG generates an $Fe(CO)_2(CN)$ synthon with Complex A as the intermediate. Note that the stereochemistry of the dangler Fe in Complex A is unclear. Isotopically labeled nuclei used in this study are shown in colors. Met = L-methionine; dAdoH = 5'-deoxyadenosine; other abbreviations are noted in the text. The spin states of the dangler Fe in Fe species are indicated as HS ($S = 2$) or LS ($S = 0$).

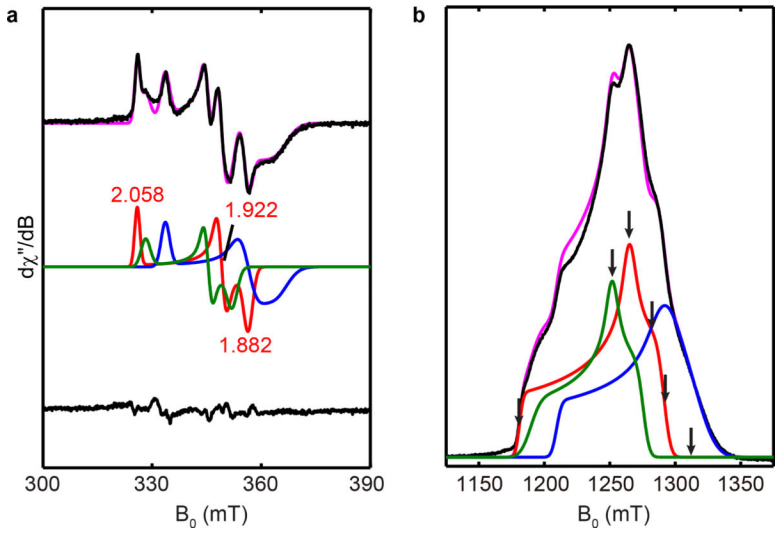

Figure 2.

Deconvolution of the HydG reaction EPR spectra. **a**, Top: X-band (9.4 GHz) CW-EPR spectrum of the 24 s HydG reaction sample (black trace), and the total simulation (magenta trace). Middle: simulation of the top black trace with three species: species **1** (Complex A, 35%, red trace), species **2**, (SAM bound $[4Fe\text{-}4S]^{+}_{RS}$ cluster, 43%, blue trace) and species **3** (unknown structure, 22%, green trace). Bottom: the difference between the experimental spectrum and the total simulation. **b**, Q-band (34 GHz) electron spin-echo detected EPR spectrum of the 24 s reaction sample (black trace) and its simulated components: species **1** (red trace), 40%; species 2 (blue trace), 31%; species **3** (green trace), 29%. The field positions used for ^{13}C Mims-ENDOR measurements are indicated by arrows (from left to right, g = 2.055, 1.940, 1.922, 1.890, 1.882 and 1.851, respectively). Parameters for X-band CW-EPR: temperature, 10 K; microwave power, 0.02 mW (non-saturating); modulation amplitude, 0.5 mT. Parameters for Q-band measurements: temperature, 10 K; $\pi/2$ = 12 ns; τ = 300 ns.

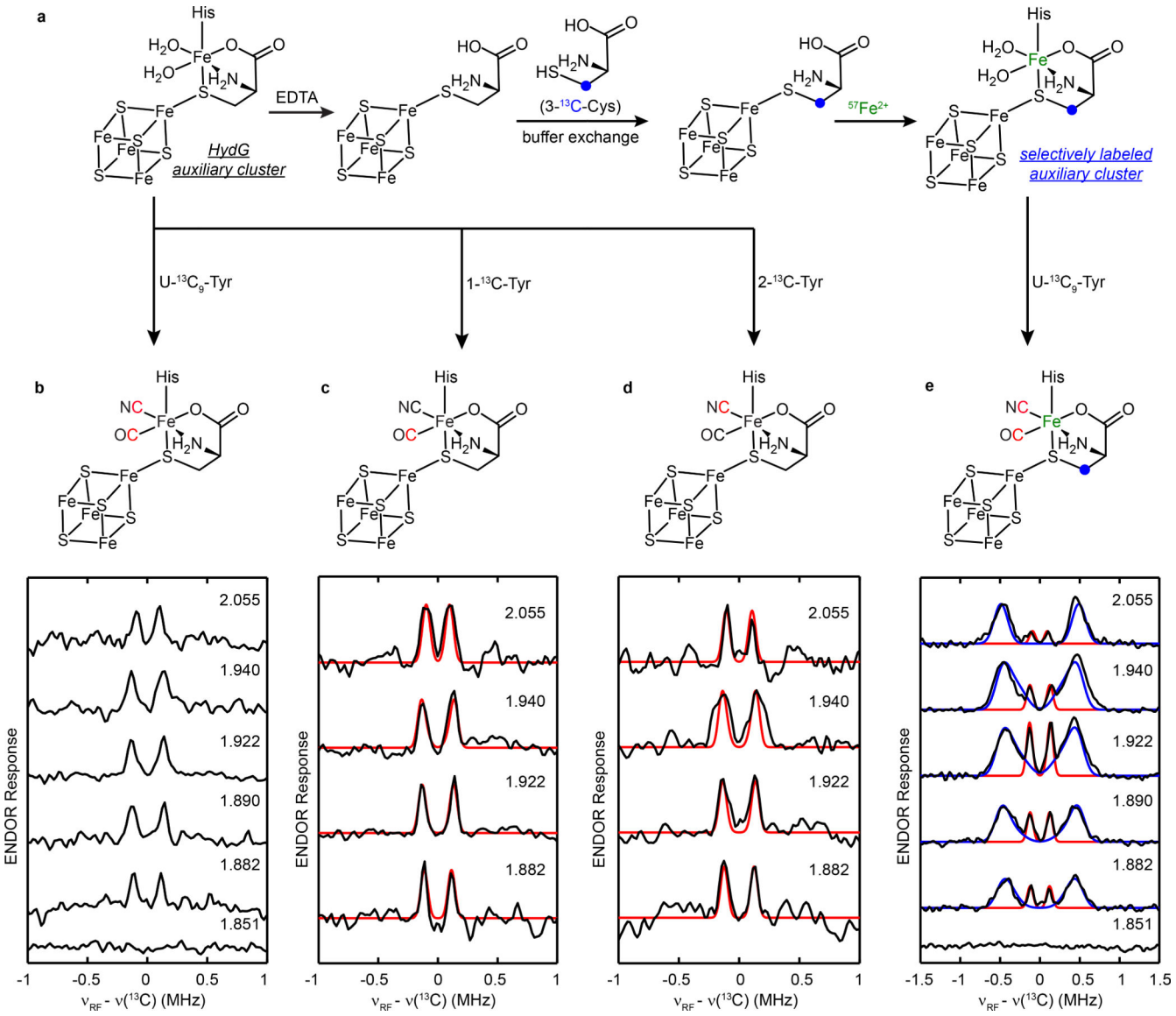

Figure 3.

^{13}C Mims-ENDOR spectra of the HydG reaction mixture generated under the standard condition. **a**, Overview of the strategies to selectively label HydG and HydG reaction intermediates. **b**-**e**, Field-dependent ^{13}C Mims-ENDOR spectra of HydG reaction mixture generated by using U-$^{13}C_9$-Tyr + natural abundance (N.A.) HydG (**b**), 1-^{13}C-Tyr + N.A. HydG (**c**), 2-^{13}C-Tyr + N.A. HydG (**d**), and U-$^{13}C_9$-Tyr + 3-$^{13}C\text{-}Cys_{bridge}$, $^{57}Fe_{dangler}$-HydG (**e**). Labeled ^{13}C nuclei are marked in red (from Tyr) and blue (from Cys). Labeled ^{57}Fe nuclei are marked in green. Parameters for Mims-ENDOR: temperature, 10K; $\pi/2$ = 12 ns; τ = 300 ns; RF pulse = 30 μs. Parameters for simulation: g = [2.058, 1.922, 1.881]; A = [0.10, 0.30, 0.27] MHz; Euler angle = [30, 30, 0]°(**c**); A = [0.15, 0.30, 0.28] MHz; Euler angle = [0, 30, 0]° (**d**); and A = [1.00, 0.20, 1.00] MHz; Euler angle = [60, 35, −60]° (**e**, blue trace). The red trace in **e** represents the total contributions from ^{13}CO and ^{13}CN HFI.

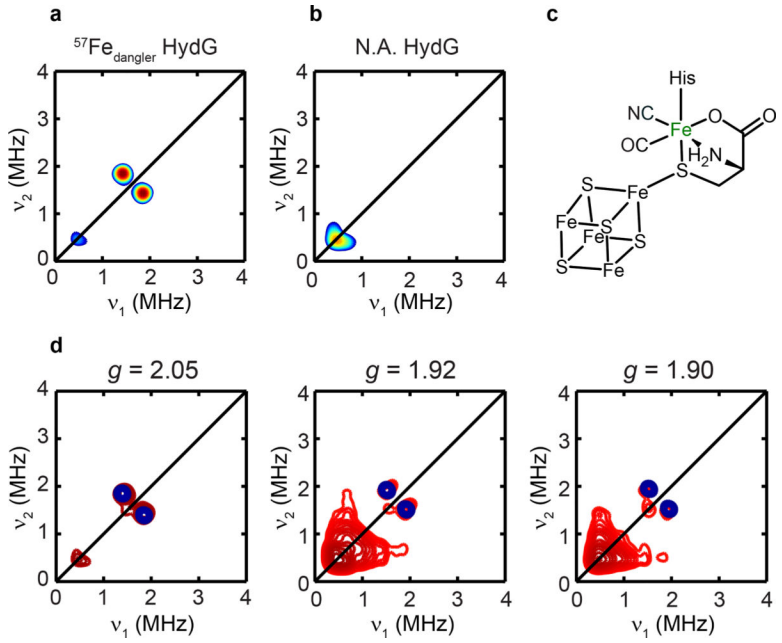

Figure 4.

^{57}Fe HYSCORE spectra of HydG reaction mixture generated under the standard condition. Q-band (34 GHz) HYSCORE spectra of Complex A with $^{57}Fe_{dangler}$ HydG (**a**) and natural abundance HydG (**b**) at $g = 2.05$. **c**, Depiction of Complex A with the labeled Fe marked in green. **d**, Field-dependent HYSCORE spectra of Complex A with $^{57}Fe_{dangler}$–labeled HydG (red contours) and the simulations (blue contours) using $g = [2.058, 1.922, 1.882]$, $A = [0.50, 0.35, 0.40]$ MHz and Euler angle = [0, 60, 0]°. Parameters for Q-band HYSCORE spectroscopy: temperature, 10 K; $\tau = 300$ ns; $\pi/2 = 12$ ns; $\pi = 24$ ns. The time increment in both dimensions was 24 ns with 180 steps.

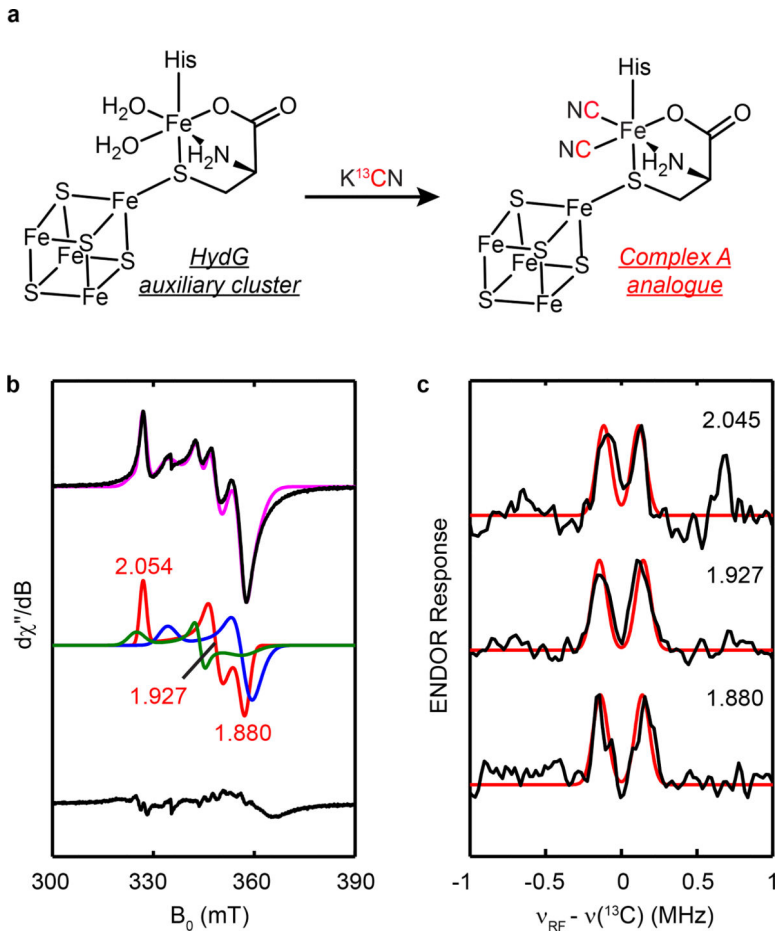

Figure 5.

Dicyano analogue of Complex A. **a**, Scheme showing the generation of the dicyano analogue. **b**, Top: CW EPR spectrum of HydG + 50 eq. KCN (black trace), and the total simulation (magenta trace). Middle: simulation of top black trace with three species (Supplementary Information): dicyano analogue (47%, red trace), SAM bound $[4Fe\text{-}4S]^{+}_{RS}$ cluster (32%, blue trace) and unknown structure (21%, green trace). Bottom: the difference between the experimental spectrum and the total simulation. **c**, Field-dependent ^{13}C Mims-ENDOR spectra (black trace) of the sample in **b**, simulated with g = [2.054, 1.927, 1.880], A = [0.20, 0.30, 0.30] MHz and Euler angle = [0, 30, 0]° (red trace). Parameters for X-band CW-EPR and Q-band ENDOR experiments were same as those in Fig. 2 and 3.

Table 1.

Comparison of weak ^{57}Fe hyperfine interactions in various Fe proteins.

^{57}Fe species	***A* ^{57}Fe (MHz)**	**[α, β, γ] (degree)**	**ref**
HydG Complex A	[0.45, 0.30, 0.50]	[0, 60, 0]	this work
Ni-A state	1.0	-	[39]
Ni-C state	0.8	-	[39]
Ni-B state	0.8	-	[40]
LipA intermediate[a]	[1.2, 1.4, 2.5]	-	[36]
	[1.3, 1.0, 0.1]	-	[36]
H_{ox}-CO Fe_d (HydA1)	[−1.7, 2.8, 2.8]	[0, 30, 90]	[38]
H_{ox}-CO Fe_d (DdH)	[2.1, 2.1, −1.7]	[0, 30, 90]	[37]

[a] Two sets of ^{57}Fe HFI were observed from a [4Fe-4S] cluster.